Viscoelastic Behavior of Thermally Treated Aqueous Xanthan Solutions in the Semidilute Concentration Regime

Henry W. Oviatt, Jr., and David A. Brant*

Department of Chemistry, University of California, Irvine, California 92717-2025

Received September 2, 1993; Revised Manuscript Received October 10, 1993®

ABSTRACT: The rheology of five fractions of the microbial polysaccharide xanthan has been studied in semidilute aqueous solution. Samples covering a 3-fold range of molecular weight ((0.46–1.20) × 10^6 g mol^{-1}) and a 3-fold range of concentration (1.0–3.0 g dL^{-1}) have been investigated. The samples were heated for 20 min at 121 °C in the presence of 0.10 M NaCl and cooled to room temperature for measurement. Xanthan samples prepared in this way exhibit large increases in steady shear viscosity, dynamic viscosity, and dynamic storage and loss moduli relative to the unheated control samples. Procedures are presented for bringing much of the data onto rather well-defined master curves that disclose clear systematic differences between the behavior of autoclaved and unheated samples and between xanthan samples of high and low molecular weight. The heat-treated xanthan samples display viscoelasticity and pseudoplasticity that rival or exceed those shown at similar concentrations by the polysaccharide hyaluronic acid (HA), widely employed in ocular surgical techniques for its desirable rheological properties. The development of HA-like rheology in xanthan is interpreted here in terms of tenuous network formation involving junction zones between xanthan chains that are based on the duplex motif of the native xanthan double strand. Under the conditions of added salt described, autoclaving at 121 °C is postulated to disrupt the native duplex, which re-forms on cooling of the highly interpenetrating semidilute polymer coils to form additional duplex network junction zones. Extreme pseudoplasticity arises from the ready disruption of these junction zones by shear. The higher molecular weight controls also exhibit many rheological characteristics in common with the autoclaved samples. These similarities are interpreted in terms of the existence of a significant proportion of nonequilibrium duplex structure, and hence more extensive network development, in the higher molecular weight controls than is present in their lower molecular weight counterparts.

Introduction

Xanthan is a regularly repeating, ionic copolysaccharide produced by the bacterium *Xanthomonas campestris*. The five-sugar repeating unit (Figure 1) consists of a dimeric backbone segment, identical with that of cellulose, to which is attached a three-sugar side chain on every second backbone sugar;[1,2] the pyruvate ketal on the mannose residue distal to the main chain and the acetyl group at C6 of the proximal mannose may not occur on every repeating unit. Xanthan is produced in significant amounts by commercial fermentation for use in a wide variety of aqueous viscosity control applications.[3] The advantageous properties of xanthan derive from the chain stiffness of its double-stranded native structure[4-7] and the capacity of the polymer to establish a weakly cross-linked gel-like network structure.[8-13]

We have reported recently that appropriate thermal processing enhances the viscoelasticity and pseudoplasticity of semidilute aqueous xanthan solutions.[14] Heating to temperatures above the characteristic temperature T_m of the xanthan order ↔ disorder transition[15-18] is postulated to disrupt the native double strands. When the system is returned to room temperature, the duplex structure is reestablished. Under concentration conditions corresponding to extensive interpenetration of polymer coils, a highly ramified network develops. The proposed network junctions, based on the native xanthan double-strand motif, impart enhanced elasticity and viscosity to the sample, but they are readily subject to disruption by shear. Accordingly, xanthan samples prepared in this way demonstrate greater pseudoplasticity than other commonly used polysaccharide viscosity control agents.[19] Only aqueous hyaluronic acid, widely used as a surgical aid in ocular surgery because of its desirable rheology,[20,21] displays comparable shear-thinning behavior.[22-24]

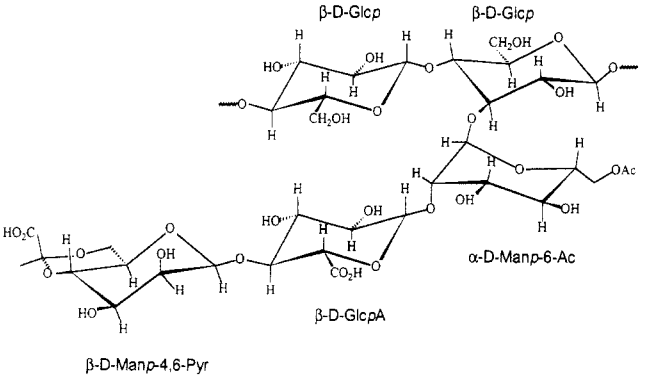

Figure 1. Structural repeating unit of xanthan.

The extent of network structure formed upon cooling semidilute aqueous xanthan following heat treatment above T_m depends on the concentration of low molecular weight salt present.[14] When salt is absent, the kinetics of the disorder → order transformation are slow,[12,15,18,25] and cooling from above T_m is less effective in producing enhanced viscoelasticity and pseudoplasticity than when salt is present. Most effective is addition of salt once cooling is completed.[14] This protocol provokes abrupt formation of double-stranded cross-links under conditions that are kinetically not conductive to annealing of the system toward the thermodynamically more stable states, which involve extensive double-strand formation but fewer cross-links effective as network junctions.[14,25,26]

It should be noted here that simple statistical thermodynamic considerations[25,26] suggest that the true equilibrium state for duplex xanthan at temperatures well below the order ↔ disorder transition temperature consists of a population of homogeneous duplex dimers in which every xanthan strand is involved in ordered duplex

* Author to whom correspondence should be addressed.
® Abstract published in *Advance ACS Abstracts*, March 15, 1994.

0024-9297/94/2227-2402$04.50/0

formation with one other strand of essentially the same length. In this state, which may be difficult to reach for kinetic reasons, no clusters of more than two xanthan chains will be present. Hence, in this limiting equilibrium condition there will be no contributions to network cross-linking from interactions that conform to the duplex motif.

Notwithstanding the rheological advantages of adding salt after cooling, we report here on samples prepared by cooling semidilute aqueous xanthan solutions that have been autoclaved at 121 °C in the presence of 0.1 M NaCl. Such samples have only marginally poorer rheological properties than those to which salt is added after cooling.[14] They have the advantage that sterile samples can be prepared, in a hypodermic syringe, for example, without further manipulation that might compromise sterility. In what follows we describe the dependence on xanthan molecular weight and concentration of the rheological properties of thermally treated semidilute (1–3 g/dL) xanthan in 0.1 M NaCl.

Experimental Section

A. Xanthan Sample Preparation. Commercial food-grade xanthan powder (Kelco Keltrol, lot no. 76735A) was used in this study. The degrees of acetyl and pyruvyl substitution of this sample are known[27] to be 0.81 and 0.59, respectively, from NMR measurements.[28] The method of continuous sonication used to reduce the molecular weight has been described previously.[14] In the present instance, 30 g of xanthan was suspended initially in 3 L of 0.1 M aqueous NaCl. Samples of ~500 mL were removed after various periods of sonication. These samples were diluted with an equal volume of distilled water, centrifuged to remove large particulates, and filtered successively through 3.0-, 1.2-, and 0.8-μm filters (Millipore HA) under pressure. Optically clear solutions resulted.

Isopropyl alcohol (IPA) was added dropwise to each filtered solution until the first appearance of a precipitate. This was removed by centrifugation at 8000 rpm for 45 min, the supernatant was decanted, and the precipitate was discarded. A second portion of IPA (100–200 mL) was added to the supernatant to precipitate the bulk of the remaining xanthan. This was removed by centrifugation, and a third addition of IPA was made to verify that all of the remaining polymer had not been precipitated in the second fraction. This operation was designed to remove the high and low molecular weight tails from the molecular weight distributions of the sonicated xanthan samples.

The second (middle) fraction was washed with IPA, compacted by centrifugation, and dried in vacuo at 40 °C overnight. The resulting hard, porous mass was easily ground to a fine powder and was stored in a desiccator containing $CaSO_4$. These samples dissolved completely within 1 h in distilled water but required slightly longer times to dissolve in 0.1 M NaCl solution. The samples were numbered 1–5; sample 1 was sonicated least and has the highest molecular weight while sample 5 was sonicated longest and has the smallest molecular weight. Residual salt and water contents of the dried powders were not measured.

B. Characterization of Samples. The weight-average molecular weights (M_w), root-mean-square radii of gyration ($\langle s^2 \rangle_z^{1/2}$), and light scattering osmotic second virial coefficients (A'_2) of samples 1–5 were measured with a Brookhaven Model BI-200SM light scattering goniometer following sample preparation and measurement techniques described previously.[29,30] All measurements were made in aqueous 0.1 M NaCl using the 488-nm radiation from an argon ion laser. A value of 0.144 mL/g was used for the differential refractive index increment.[5] A summary of the characteristics of samples 1–5 appears in Table 1.

C. Rheological Measurements. Solutions for rheological measurements were prepared by dissolving the appropriate mass of dried, purified xanthan powder in 0.1 M NaCl in a scintillation vial containing a magnetic stirring bar. Concentrations are expressed in g/dL (grams of polymer per deciliter of solvent); residual water content of the powdered samples (estimated to be 10%) was not taken into account in expressing polymer concentrations. Scintillation vials were sealed with polyethylene-lined screw caps. The resulting solutions were split into two portions. One portion was placed in a 3-dram vial with a poly(tetrafluoroethylene)-lined screw cap, and the second portion was left in the scintillation vial. The portions in 3-dram vials were autoclaved (Sybron/Barnstead Model C2250) at 121 °C for a 20-min cycle. The portions not autoclaved are referred to in what follows as the control samples. Both the control and autoclaved portions were refrigerated until tested. Most samples were prepared 1 day prior to measurement.

Table 1. Physical Characteristics[a] of Xanthan Samples Used in This Study

sample	sonication time (h)	$10^{-6}M_w$ (g mol^{-1})	$\langle s^2 \rangle_z^{1/2}$ (nm)	$10^4 A'_2$ (mL mol g^{-2})
1	0.17	1.20	161	5.72
2	0.44	1.10	149	5.24
3	0.89	0.630	100	5.20
4	1.17	0.574	92	5.56
5	2.00	0.458	79	6.40

[a] Weight-average molecular weights (M_w), root-mean-square z-average radii of gyration ($\langle s^2 \rangle_z^{1/2}$), and osmotic second virial coefficients (A'_2) from light scattering. See text for pyruvate and acetate contents.

Measurements were performed on a Rheometrics RFS II fluids spectrometer with two transducers (100 g cm for steady shear and 10 g cm for dynamic (oscillatory) experiments). Calibration of the transducers was checked periodically. A cone-and-plate tool with a cone angle of 0.02 rad and a diameter of 50 mm was used for all tests. The temperature was controlled at 23 °C with a circulating bath. The less viscous samples were loaded by pouring the sample onto the lower plate. The more viscous samples required loading the lower plate with a spatula. After the sample was loaded, the normal force reading on the instrument was allowed to relax. If the normal force failed to reach zero, it was adjusted to zero by raising the cone slightly. In all cases a gap between the cone and plate of 0.03 mm or less was used unless otherwise noted. Dynamic measurements on the autoclaved samples were run with a strain of 1%. For the least viscous control samples a strain of 5% was used to improve the sensitivity. All dynamic measurements were made within the linear viscoelastic regime.[31] Measurements on a given sample were reproducible in successive ascending and descending frequency or shear rate sweeps. This indicates that significant solvent evaporation did not occur in the course of the reported measurements, all of which were conducted at room temperature.

The Rheometrics data files were transferred to a personal computer and the results plotted with a commercial spreadsheet program. Data sets are named to denote the technique of measurement, sample treatment, and concentration. Dynamic runs are designated FS (frequency sweep), while steady shear experiments are designated RS (rate sweep). A suffix A or C is appended to identify the sample as autoclaved or control, respectively. The concentration is then appended in g/dL (or, equivalently, in % w/v). For example, a frequency sweep data set for control sample 3 at 1.5% is designated FSC3-1.5, and a steady shear experiment on the corresponding autoclaved sample is designated RSA3-1.5. When the concentration is omitted (e.g., FSC2), the (frequency sweep) data for all concentrations (of control sample 2) are under consideration. Five concentrations (1.0, 1.5, 2.0, 2.5, and 3.0%) were investigated for each autoclaved and control sample.

D. Method of Extracting η_0 and η^*_0. The steady shear viscosity at vanishing shear rate, η_0, and the modulus of the dynamic (complex) viscosity at vanishing frequency, η^*_0, are required to convert the rheological data to reduced form.[31,32] Pronounced shear thinning of the present xanthan solutions, especially after autoclaving,[14] prevents direct measurements of η_0 in the Newtonian region of the flow curve. Consequently, η_0 must be estimated by extrapolation from data at higher shear rates. It is similarly necessary to obtain an estimate of η^*_0 by extrapolation. We have made the required extrapolations by plotting the observed values of η and η^* against measured torque, τ, as discussed by Vinogradov and Malkin.[32] For the control samples, and especially for the autoclaved samples, these plots are curved. Linear regression fits to the 4–6 points at lowest τ

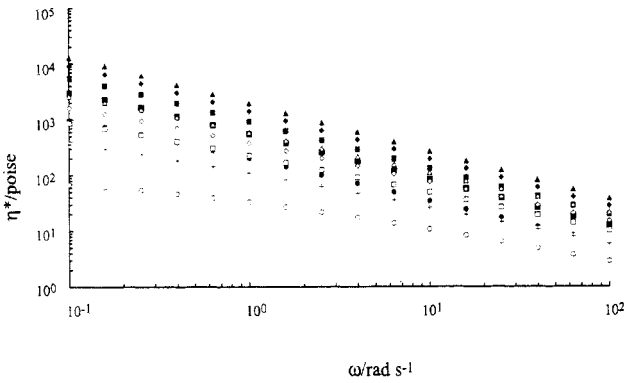

Figure 2. Dynamic viscosity η^* in poise plotted versus angular frequency ω in rad/s for sample 1 (autoclaved and control) at all five concentrations: FSA1-1.0 (●), FSA1-1.5 (■), FSA1-2.0 (▪), FSA1-2.5 (♦), FSA1-3.0 (▲), FSC1-1.0 (○), FSC1-1.5 (+), FSC1-2.0 (□), FSC1-2.5 (◊), FSC1-3.0 (△).

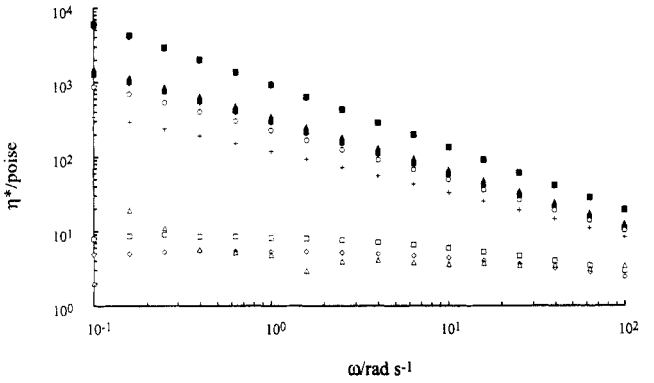

Figure 3. Dynamic viscosity η^* in poise plotted versus angular frequency ω in rad/s for samples 1–5 (autoclaved and control) at a concentration of 2%: FSA1-2.0 (●), FSA2-2.0 (■), FSA3-2.0 (▪), FSA4-2.0 (♦), FSA5-2.0 (▲), FSC1-2.0 (○), FSC2-2.0 (+), FSC3-2.0 (□), FSC4-2.0 (◊), FSC5-2.0 (△).

permit, however, extrapolations to η_0 and η^*_0 with correlation coefficients $r \approx 0.99$. More conventional plots of η or η^* versus shear rate, $\dot{\gamma}$, or frequency, ω, respectively, have more curvature than plots against τ and are more difficult to extrapolate. Likewise, extrapolation of G''/ω to vanishing frequency to obtain η_0[31] was less successful than extrapolation of η against τ, suggesting that the viscous modulus, G'', does not approach a limiting slope in the experimental frequency range. The efficacy of the present procedure for obtaining η_0 and η^*_0 is demonstrated by the success, reported below, in constructing master curves from the data.

E. Preparation of Master Curves. Some of the rheological data are collected on master curves by reducing or adjusting the observables using well-established procedures.[31,32] The elastic modulus, G', and the solvent-corrected viscous modulus, $G'' - \omega\eta_s$, from the oscillatory measurements were reduced to dimensionless variables by dividing each by the Rouse coefficient cRT/M. Here ω is the frequency (rad/s), η_s is the solvent viscosity (poise), M is the number-average molecular weight (g/mol), here approximated by M_w, c is the polymer concentration (g/mL), R is the gas constant (ergK^{-1} mol^{-1}), and T is the temperature (K). The reduced variables $G'_r = G'M/cRT$ and $G''_r = (G'' - \omega\eta_s)M/cRT$ are plotted against an adjusted frequency ω_a, defined by $\omega_a = \omega(\eta^*_0/\eta^*_{0,ref})$, where η^*_0 is the zero-frequency dynamic viscosity of the sample in question and $\eta^*_{0,ref}$ refers to the zero-frequency dynamic viscosity of the same sample at some reference concentration, chosen here to be 3%. This arbitrary choice of reference concentration was made to take advantage of the precision of the measurements made at the highest concentration (3%). Explicit inclusion of polymer concentration in the adjustment factor for ω_a, which might be suggested on some grounds,[31,32] was far less successful in producing tight master curves for G'_r and G''_r. Dimensionless reduced steady shear viscosities, $\eta_r = \eta/\eta_0$, were plotted against dimensionless reduced shear rate $\dot{\gamma}_r = \dot{\gamma}\tau_1$, and dimensionless reduced dynamic viscosities $\eta^*_r = \eta^*/\eta^*_0$ were plotted against dimensionless reduced frequency $\omega_r = \omega\tau_1$. Here reduction of $\dot{\gamma}$ and ω is accomplished using the longest Rouse relaxation time $\tau_1 \approx \eta_0 M/cRT$. All data are plotted in conventional log–log fashion.

Results and Discussion

A. Frequency Dependence of Dynamic Viscosity. The dynamic viscosity, η^*, is plotted as a function of frequency, ω, in Figure 2 for sample 1 at five concentrations. Both FSA1 and FSC1 appear on the plot. In general, the autoclaved samples show a 5–10-fold greater dynamic viscosity than the corresponding controls, with the larger ratios occurring at the lower frequencies studied. The greater pseudoplasticity of the autoclaved samples is made apparent by observing that the curve for the 3% control sample is intersected by the curves for the three lower concentration autoclaved samples as ω increases. For both FSA1 and FSC1 η^* increases smoothly with increasing concentration.

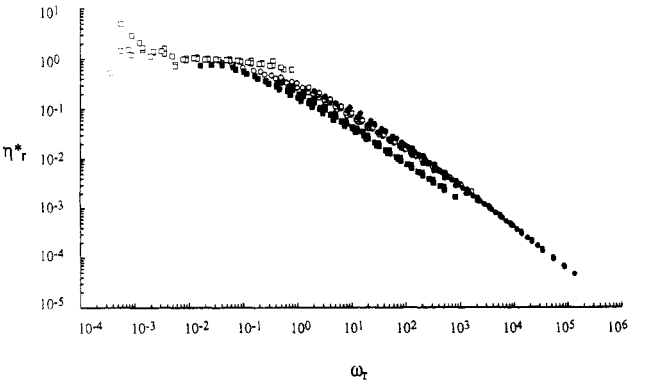

Figure 4. Reduced dynamic viscosity η^*_r plotted versus reduced frequency ω_r for samples 1 and 5 (autoclaved and control) at all five concentrations: FSA1 (●), FSA5 (▪), FSC1 (○), FSC5 (□).

Figure 3 shows the molecular weight dependence of η^* for the five autoclaved and control samples, all at a concentration of 2%. In this figure the lower molecular weight (LMW, $M_w \leq 0.63 \times 10^6$ g/mol) control samples 3, 4, and 5 show nearly Newtonian behavior across the frequency range, while the higher molecular weight (HMW, $M_w \geq 1.10 \times 10^6$ g/mol) control samples 1 and 2 exhibit pseudoplastic behavior. The pseudoplasticity of the HMW control samples mimics that often reported for solutions of xanthan that have not been sonicated or heat treated.[12,13,33] After autoclaving, the five samples all show shear-thinning behavior and produce two families of η^* curves separated by about half an order of magnitude. The lower three curves, corresponding to the LMW samples which exhibit Newtonian behavior in the controls, are now seen nearly to superimpose with a strong frequency dependence. At the lowest frequency studied, these samples have increased in η^* by 2 orders of magnitude as a result of thermal treatment. The two HMW samples have increased in η^* by 1 order of magnitude at low frequency and exhibit a stronger dependence on ω than before autoclaving. The latter two curves are essentially indistinguishable in Figure 3. Figures 2 and 3 illustrate the breadth of viscoelastic behavior found in control and autoclaved xanthan solutions for the ranges of molecular weight and concentration investigated here. In what follows samples 1 and 5 will be used to illustrate the behavior of the HMW and LMW samples, respectively.

Figure 4 is a plot of the reduced dynamic viscosity, η^*_r, versus dimensionless frequency, ω_r, for autoclaved and control samples 1 and 5 at all concentrations investigated. The reduced data for FSA1 and FSC1 appear to lie on a common curve, which is frequency dependent throughout

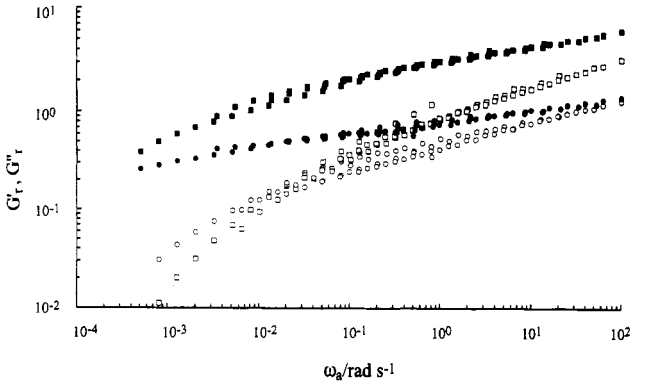

Figure 5. Reduced dynamic moduli G'_r (squares) and G''_r (circles) plotted versus adjusted frequency ω_a in rad/s for sample 1 (autoclaved and control) at all five concentrations: FSA1 (■,●), FSC1 (□,○).

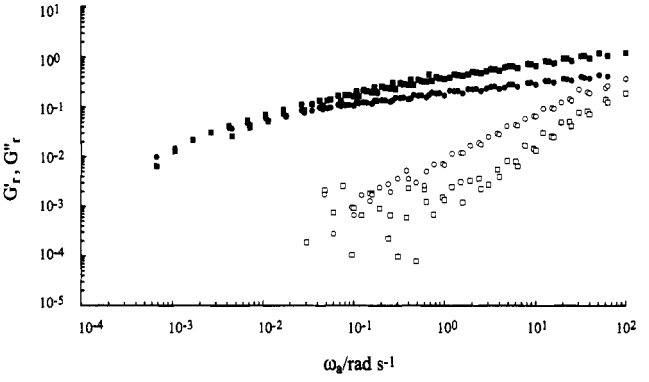

Figure 6. Reduced dynamic moduli G'_r (squares) and G''_r (circles) plotted versus adjusted frequency ω_a in rad/s for sample 5 (autoclaved and control) at all five concentrations: FSA5 (■,●), FSC5 (□,○).

the experimental range. For FSA5 and FSC5 a single master curve for autoclaved and control samples does not result. The scatter in the terminal (low frequency) region for FSC5 is due to the relatively small magnitude of η^* for this sample and the resulting lack of precision in the measurement. Samples FSA5 show a strong frequency dependence of η_r, even at the lowest concentrations, while for FSC5 little frequency dependence is apparent at any concentration investigated. The curves for FSA5 and FSC5 clearly do not correspond to the same functional relationship between η^* and ω_r. From Figure 4 it thus appears that the essential viscoelastic character of xanthan solutions with $M_w > 1 \times 10^6$ g/mol is not changed by autoclaving, whereas the lack of superimposibility of the FSA5 and FSC5 data suggests that a fundamental structural change has occurred upon autoclaving the samples with $M_w < 6 \times 10^5$ g/mol.

B. Reduced Elastic and Viscous Moduli. Figures 5 and 6 show plots of the reduced elastic and viscous moduli, G'_r and G''_r, versus adjusted frequency, ω_a, for samples 1 and 5, respectively. Data for all concentrations are included. The autoclaved samples (filled symbols) appear to form "tighter" master curves than the control samples (empty symbols). The greater scatter in the data for the control samples, especially for the LMW samples, arises in part from the lower signal to noise for the low-modulus samples. The trends are clear: There is a large increase in moduli associated with the autoclaved samples in comparison with the corresponding control samples, and the reduced moduli of the autoclaved samples show a smaller frequency dependence than do those of the control samples. At the highest reduced frequencies explored, the values of G'_r and G''_r for the controls approach those of the heat-treated samples.

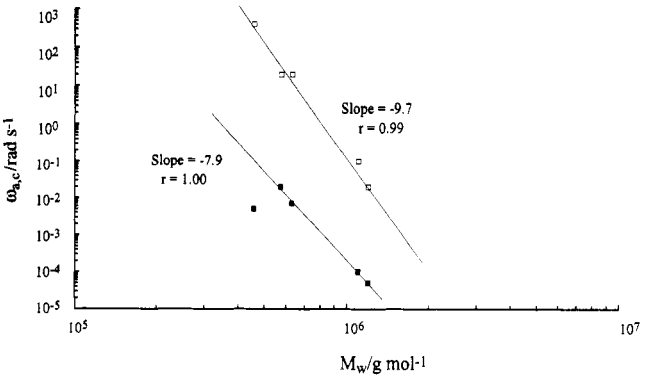

Figure 7. Adjusted crossover frequency $\omega_{a,c}$ in rad/s plotted versus weight-average molecular weight M_w in g/mol for samples 1–5 (autoclaved and control) at all five concentrations: FSA (■), FSC (□).

There are again clear differences between the HMW samples (Figure 5) and the LMW samples (Figure 6). For the HMW autoclaved samples FSA1, $G'_r > G''_r$ over the entire adjusted frequency range explored. For the LMW autoclaved samples FSA5, G'_r crosses G''_r within the experimental frequency range. The HMW control samples FSC1 also show a crossover of G'_r and G''_r, but for the LMW control samples FSC5, this crossover is not observed or occurs only at the highest frequencies studied. Finally, the moduli of the LMW samples are more sensitive to the effects of autoclaving than are those of the HMW samples.

The elastic plateau region, with onset at frequency $\omega_{a,c}$ where G'_r first exceeds G''_r, occurs for the autoclaved HMW samples below the experimental range of ω_a. For the autoclaved LMW samples, $\omega_{a,c}$ occurs at ω_a values which decrease with increasing M_w within the experimental range. Thus, all autoclaved samples are within the elastic plateau region of viscoelastic behavior, at least at the upper end of the experimental frequency range. The values of $\omega_{a,c}$ for the control samples are appreciably larger than those for the corresponding autoclaved samples, and, consequently, G'_r and G''_r are more frequency dependent than their autoclaved counterparts throughout much of the experimental frequency range. Nevertheless, the HMW control samples display behavior in the viscoelastic plateau region at the higher experimental frequencies. For the LMW controls $\omega_{a,c}$ corresponds roughly to the upper end of the experimental range of ω_a.

The points, $\omega_{a,c}$, at which G'_r and G''_r cross on the adjusted frequency axis, as determined by visual inspection (and extrapolation beyond the experimental range when required) of the G'_r and G''_r versus ω_a data, are plotted in Figure 7 against M_w. Here the autoclaved samples FSA and control samples FSC produce two separate lines. The slope for the autoclaved samples is −7.9, while that for the controls is −9.7, as determined by regression analysis. The datum for FSA5 lies off the line for the autoclaved samples, presumably because of a malfunction in the autoclave, which caused the sample to be heated longer than 20 min. This point was not included in the regression analysis.

The power law correlation between $\omega_{a,c}$ and M_w demonstrated in Figure 7 is strong. That the $\omega_{a,c}$ curve for the autoclaved samples lies toward lower frequencies than that for the controls indicates clearly that the network-stabilizing junction zones in the autoclaved samples have longer mean lifetimes than those in the corresponding control samples. For both sets of samples these lifetimes increase with increasing molecular weight, but the junction zone lifetimes of the control samples are more strongly dependent on molecular weight than are those of the autoclaved samples.

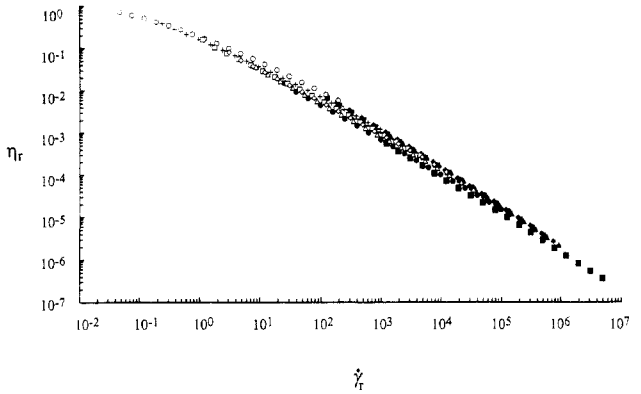

Figure 8. Reduced steady shear viscosity η_r plotted versus reduced shear rate $\dot{\gamma}_r$ for sample 1 (autoclaved and control) at all five concentrations: RSA1-1.0 (●), RSA1-1.5 (■), RSA1-2.0 (▪), RSA1-2.5 (♦), RSA1-3.0 (▲), RSC1-1.0 (○), RSC1-1.5 (+), RSC1-2.0 (□), RSC1-2.5 (◇), RSC1-3.0 (△).

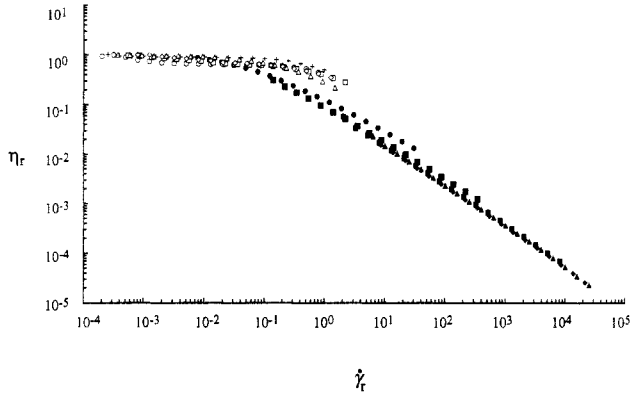

Figure 9. Reduced steady shear viscosity η_r plotted versus reduced shear rate $\dot{\gamma}_r$ for sample 5 (autoclaved and control) at all five concentrations: RSA5-1.0 (●), RSA5-1.5 (■), RSA5-2.0 (▪), RSA5-2.5 (♦), RSA5-3.0 (▲), RSC5-1.0 (○), RSC5-1.5 (+), RSC5-2.0 (□), RSC5-2.5 (◇), RSC5-3.0 (△).

If we assume that the weak xanthan network characteristic of the high-frequency elastic plateau can be described by elementary elasticity theory, then the elastic modulus is given by $G^\circ_N = g_N \nu_e RT$, where g_N is a factor close to unity, ν_e is the density of entanglement network strands, and RT has the usual meaning. Multiplying both sides by M_w, using the relation $\nu_e = c/M_e$, and rearranging yield the expression $M_w/M_e = G^\circ_N M_w/cRT$, where M_e is the mean molecular weight of chains connecting junction zones. Thus, from the dimensionless elastic modulus in the plateau region an estimate of M_w/M_e can be obtained.[34]

Using the maximum value observed for the reduced elastic modulus within the experimental frequency range yields $M_w/M_e \approx 5$ for the HMW autoclaved samples, while M_w/M_e for the LMW autoclaved samples is close to unity. Because even the HMW control samples have scarcely achieved elastic plateau behavior at the upper end of the experimental frequency range, no estimate of M_w/M_e has been attempted for the control samples. This measure of the number of junction zones per polymer chain suggests that autoclaved xanthan samples in the experimental concentration range must have $M_w \geq 5 \times 10^5$ g/mol before effective network structure exists in the experimental frequency range. This conclusion is, however, decidely contrary to the dominant impression left by our observations: The weak gel structure is well developed in autoclaved samples of the LMW xanthan, even though still larger elastic and viscous moduli can be achieved with higher molecular weight samples.

C. Reduced Steady Shear Viscosity. The reduced steady shear viscosity, η_r, is plotted against the reduced shear rate, $\dot{\gamma}_r$, for samples 1 and 5 in Figures 8 and 9, respectively. The autoclaved and control samples for each molecular weight are shown on the same plot for all concentrations. Just as for the dynamic viscosity, different behavior is seen for the LMW and HMW samples. The data for autoclaved and control HMW samples define a single, reasonably tight master curve at each molecular weight (Figure 8). The shape of the shear rate dependence is essentially the same for both types of samples, but the autoclaved samples are shifted, at a given concentration, toward higher $\dot{\gamma}_r$. Only for the least concentrated control samples is an approach to Newtonian behavior evident in Figure 8.

In contrast, efforts to construct a single master curve for autoclaved and control LMW samples in Figure 9 are less successful. Here, for xanthan of a given molecular weight, the autoclaved samples define a reasonably tight common curve that shows little tendency to approach the Newtonian plateau for any concentration studied. On the other hand, the control samples, especially those that are less concentrated, are in the Newtonian regime in the lower range of reduced shear rates investigated. The curve for the control samples is displaced vertically from that of the autoclaved samples in the range of reduced shear rate where the two curves overlap, and they do not appear to conform to the same functional relationship.

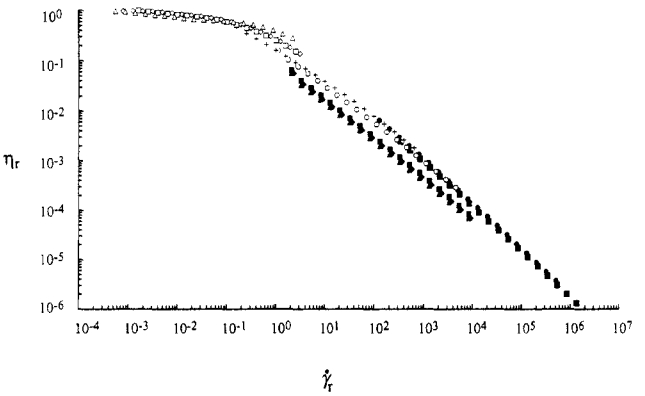

Figure 10. Reduced steady shear viscosity η_r plotted versus reduced shear rate $\dot{\gamma}_r$ for samples 1–5 (autoclaved and control) at a concentration of 2.0%: RSA1-2.0 (●), RSA2-2.0 (■), RSA3-2.0 (▪), RSA4-2.0 (♦), RSA5-2.0 (▲), RSC1-2.0 (○), RSC2-2.0 (+), RSC3-2.0 (□), RSC4-2.0 (◇), RSC5-2.0 (△).

Figure 10 displays η_r as a function of reduced shear rate, $\dot{\gamma}_r$, for the 2% solutions of all five samples, autoclaved and control. This attempt to create a master curve for xanthan samples of differing molecular weights at the same concentration succeeds for HMW samples, but, as usual, for the LMW samples separate master curves result for autoclaved and control samples. Taken together, Figures 4 and 8–10 show that the reduction procedures used here can bring the steady shear and dynamic viscosity data for semidilute xanthan solutions at different concentrations and different xanthan molecular weights onto a fairly well-defined master curve, provided all of the samples being compared have been prepared according to a common protocol. Adjustments in concentration produce, in general, somewhat tighter master curves than adjustments in molecular weight. (Compare Figures 8–10.) For the HMW samples, however, both control and autoclaved samples fall effectively on the same master curve.

The autoclaved samples, especially, show very strong shear-thinning behavior. Linear, power law, portions of the η_r versus $\dot{\gamma}_r$ curves (e.g., Figures 8–10) have a slope approaching −0.90, a value considerably larger than that

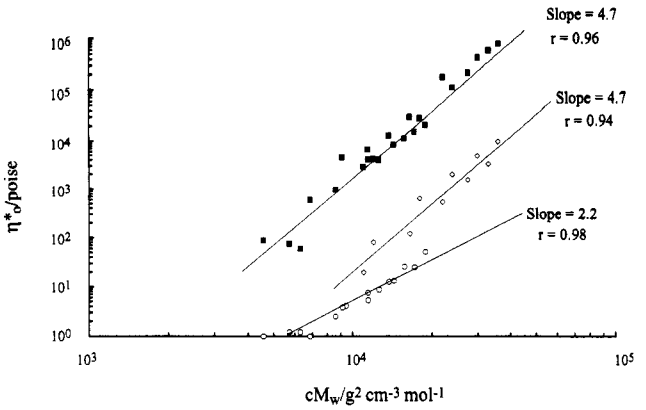

Figure 11. Zero-frequency dynamic viscosity η^*_0 in poise plotted against the product of concentration c in g/mL and weight-average molecular weight M_w in g/mol for samples 1–5 at all five concentrations: FSA (■), HMW FSC (□), LMW FSC (○).

observed for most other polysaccharides.[19] Power law portions of plots of η^*_r versus ω_r are equally steep (Figure 4). For the LMW control samples $\eta^*(\omega) \approx \eta(\dot{\gamma})$, and the Cox–Merz rule is satisfied,[35] whereas for the autoclaved samples and the HMW controls $\eta^*(\omega) > \eta(\dot{\gamma})$.[14] In regard to shear thinning, the autoclaved xanthan solutions resemble the hyaluronic acid preparations used in viscosurgery.[14] The marked pseudoplasticity of the autoclaved xanthan solutions clearly arises from the fragility of the weak network structure that is enhanced by autoclaving. Occurrence of a weak gel network in xanthan, subject to disruption by shearing forces, has frequently been noted in the past.[8–13]

The clear approach to Newtonian behavior shown by the LMW control samples in Figures 9 and 10 has not often been observed in previous studies of aqueous xanthan, even that which has not been heat treated. We attribute this unusual behavior, first, to the relatively low molecular weight of the LMW samples and, second, to our supposition that these highly sonicated samples are well ordered in the sense that they contain a high proportion of homogenous duplex dimers and consequently display a much less ramified tenuous network structure.

D. Dependence of η^*_0 on Concentration and Molecular Weight. In Figure 11 η^*_0 is plotted against the Bueche segment contact parameter cM_w, which measures the number of intermolecular contacts per polymer chain.[34] Similarities between the HMW controls and the autoclaved samples again appear. Here all of the autoclaved samples, covering nearly a 3-fold range of molecular weight and a 3-fold range of concentration, define a single reasonably tight curve with slope 4.7 (correlation coefficient $r = 0.96$). A second curve with the same slope ($r = 0.94$) is formed by the HMW controls, whereas the LMW controls describe a third line with slope 2.2 ($r = 0.98$). The limiting steady shear viscosity, η_0, shows similar behavior when plotted in this fashion.

Plots of this sort typically display a change of slope near a critical value of the segment contact $(cM_w)^*$ or coil overlap $(c[\eta])^*$ parameter. For most polymers, including polysaccharides,[36] slopes of 1.2–1.4 are found below the critical value and slopes of 3.3–3.7 are found above the critical value.[34] Cuvelier and Launay[13] identify three ranges of concentration with different scaling exponents for an aqueous xanthan sample with $[\eta] = 49.3$ dL/g. Below $c[\eta] = 1.5$ a typical dilute solution exponent (1.25) is observed, but above $c[\eta] = 5.4$ the slope is unusually high (4.2), as confirmed by Milas et al.[37] This large exponent is similar to that reported here for the autoclaved samples and the HMW controls. In the intermediate range $1.5 \leq c[\eta] \leq 5.4$ Cuvelier and Launay observe a slope of 2.1, in close agreement with that found here for the LMW control samples.

The observed strong correlation of η^*_0 with the Bueche segment contact parameter is consistent with current understanding about the nature of the transient network junction zones in semidilute aqueous xanthan solutions. The very large scaling exponent above the critical range of cM_w suggests, however, that the network junctions in these semidilute xanthan solutions differ from the simple physical entanglements thought to engender viscoelasticity in most concentrated polymer solutions or melts.

Conclusions

We have recently interpreted the rheological consequences of autoclaving semidilute aqueous xanthan solutions in terms of the formation of additional junction zones between xanthan chains based on the duplex motif of the native xanthan double strand.[14] Under the conditions of added salt described here, autoclaving at 121 °C is postulated to disrupt the native duplex, which re-forms on cooling of the highly interpenetrating semidilute polymer coils to form additional duplex network junction zones. We recall here the simple statistical thermodynamic model described in the Introduction,[25,26] which suggests that the true equilibrium state for duplex xanthan well below T_m consists of a population of homogeneous duplex dimers without extensive cross-linked network formation.

With this model in mind, we interpret the observed differences between the HMW and LMW samples as follows: It is postulated that the more highly degraded, lower molecular weight samples produced as a result of extensive sonication contain a higher proportion of ordered duplex dimer structure than do the higher molecular weight samples. These duplex dimers result (1) from the effects of chain scission in the ultrasonic shear field[38] and (2) from annealing of duplex structure that occurs during sonication. To the extent that xanthan duplex structure is confined to duplex dimers, network junctions based on the duplex motif will be diminished. (Of course other sorts of network junctions, e.g., nonspecific hydrogen bonding and cation-mediated interactions,[8,10,11] may also be present in xanthan samples, but the postulated duplex junction zones appear sufficient to explain the observations reported here.) In this picture the less sonicated HMW samples are postulated to be further from the equilibrium state, which is rendered kinetically more inaccessible by the higher molecular weight of the xanthan chains. These samples are therefore imagined to contain more extensive network structure before autoclaving. Hence, although autoclaving clearly increases the extent of ramified structure, enough such structure exists before autoclaving to render the behavior of HMW control samples very similar to that of the autoclaved samples.

Acknowledgment. This work was supported by NIH Grant No. GM 33062 to D.A.B.

References and Notes

(1) Jansson, P.-E.; Kenne, L.; Lindberg, B. *Carbohydr. Res.* **1975**, *45*, 275–282.
(2) Melton, L. D.; Mindt, L.; Rees, D. A.; Sanderson, G. R. *Carbohydr. Res.* **1976**, *46*, 245–257.
(3) Kennedy, J. F.; Bradshaw, I. J. *Prog. Ind. Microbiol.* **1984**, *19*, 319–371.
(4) Holzwarth, G. *Carbohydr. Res.* **1978**, *66*, 173–186.
(5) Paradossi, G.; Brant, D. A. *Macromolecules* **1982**, *15*, 874–879.
(6) Sato, T.; Norisuye, T.; Fujita, H. *Macromolecules* **1984**, *17*, 2696–2700.
(7) Stokke, B. T.; Brant, D. A. *Biopolymers* **1990**, *30*, 1161–1181.

(8) Ross-Murphy, S. B.; Morris, V. J.; Morris, E. R. *Faraday Symp. Chem. Soc.* **1983**, *18*, 115–129.
(9) Lim, T.; Uhl, J. T.; Prud'homme, R. K. *J. Rheol.* **1984**, *28*, 367–379.
(10) Morris, E. R. In *Gums and Stabilizers for the Food Industry, 2*; Phillips, G. O., Williams, P. A., Wedlock, D. J., Eds.; Pergamon Press: Oxford, England, 1984; Vol. 2, pp 57–78.
(11) Richardson, R. K.; Ross-Murphy, S. B. *Int. J. Biol. Macromol.* **1987**, *9*, 257–264.
(12) Rochefort, W. E.; Middleman, S. *J. Rheol.* **1987**, *31*, 337–369.
(13) Cuvelier, G.; Launay, B. *Carbohydr. Polym.* **1986**, *6*, 321–333.
(14) Oviatt, H. W., Jr.; Brant, D. A. *Int. J. Biol. Macromol.* **1993**, *15*, 3–10.
(15) Holzwarth, G. *Biochemistry* **1976**, *15*, 4333–4339.
(16) Morris, E. R.; Rees, D. A.; Young, G.; Walkinshaw, M. D.; Darke, A. *J. Mol. Biol.* **1977**, *110*, 1–16.
(17) Paoletti, S.; Cesàro, A.; Delben, F. *Carbohydr. Res.* **1983**, *123*, 173–178.
(18) Norton, I. T.; Goodall, D. M.; Frangou, S. A.; Morris, E. R.; Rees, D. A. *J. Mol. Biol.* **1984**, *175*, 371–394.
(19) Morris, E. R. *Carbohydr. Polym.* **1990**, *13*, 85–96.
(20) *Viscoelastic Materials*: *Basic Science and Clinical Applications*; Rosen, E. S., Ed.; Pergamon Press: New York, 1989.
(21) Liesegang, T. J. *Surv. Ophthalmol.* **1990**, *34*, 268–293.
(22) Gibbs, D. A.; Merrill, E. W.; Smith, K. A. *Biopolymers* **1968**, *6*, 777–791.
(23) Morris, E. R.; Rees, D. A.; Welsh, E. J. *J. Mol. Biol.* **1980**, *138*, 383–400.
(24) Yanaki, T.; Yamaguchi, T. *Biopolymers* **1990**, *30*, 415–425.
(25) Hacche, L. S.; Washington, G. E.; Brant, D. A. *Macromolecules* **1987**, *20*, 2179–2187.
(26) Washington, G. E. Ph.D. Thesis, University of California, Irvine, 1987.
(27) Bishay, I. E. Ph.D. Thesis, University of California, Irvine, 1989.
(28) Rinaudo, M.; Milas, M.; Lambert, F.; Vincendon, M. *Macromolecules* **1983**, *16*, 816–819.
(29) Talashek, T. A.; Brant, D. A. In *Frontiers in Carbohydrate Research—1*: *Food Applications*; Millane, R. P., BeMiller, J. N., Chandrasekaran, R., Eds.; Elsevier Applied Science Publishers: London, 1989; pp 271–288.
(30) Urbani, R.; Brant, D. A. *Carbohydr. Polym.* **1989**, *11*, 169–191.
(31) Ferry, J. D. *Viscoelastic Properties of Polymers*, 3rd ed.; John Wiley and Sons: New York, 1980.
(32) Vinogradov, G. V.; Malkin, A. Y. *Rheology of Polymers*; Springer-Verlag: New York, 1980.
(33) Richardson, R. K.; Ross-Murphy, S. B. *Int. J. Biol. Macromol.* **1987**, *9*, 250–256.
(34) Graessley, W. W. *Adv. Polym. Sci.* **1974**, *16*, 1–179.
(35) Cox, W. P.; Merz, E. H. *J. Polym. Sci.* **1958**, *28*, 619–626.
(36) Morris, E. R.; Cutler, A. N.; Ross-Murphy, S. B.; Rees, D. A.; Price, J. *Carbohydr. Polym.* **1981**, *1*, 5–21.
(37) Milas, M.; Rinaudo, M.; Tinland, B. *Polym. Bull.* **1985**, *14*, 157–164.
(38) Basedow, A. M.; Ebert, K. H. *Adv. Polym. Sci.* **1977**, *22*, 83–148.